TECNIACÚSTICA
CUENCA 2023

ACCURACY AND PERFORMANCE TESTS OF A WIRELESS GEOREFERENCED NOISE SENSOR FOR MOBILE NOISE SAMPLING

G. Quintero (Guillermo Quintero Perez) [1*]
A. Balastegui (Andreu Balastegui Manso)[1]
J. Romeu (Jordi Romeu Garbi)[1]

[1]Laboratory of Acoustics and Mechanical Engineering (LEAM), Polytechnic University of Catalonia, Colom 11, Terrassa, Barcelona, 08222, Spain

ABSTRACT

Wireless Sensor Networks (WSN) have been expanded due, among many other things, to the advances in technology and the cost reductions of electronic components, which allows to produce low-cost and low-power sensor nodes. With the aim of creating a WSN for automatic noise mapping, this paper evaluates the acoustical performance of an environmental noise sensor node for mobile sampling made-out of low-cost components. The sensor is composed of a low-power microcontroller together with a MEMS microphone, a Global Navigation Satellite System (GNSS) and a Low Power Wide Area (LPWA) wireless module. Acoustical tests were carried out to validate the sensor accuracy which could be compared to a Class 2 Sound Level Meter for L_{eq}, L_{Aeq} and one-third octave band spectrum (63 Hz - 10 kHz). Moreover, signal processing, data management, low-power modes, among other tasks refinement, showed that the power consumption can be improved considerably.

Keywords – IoT, Wireless noise sensor, Low-power sensor, Mobile noise mapping

1. INTRODUCTION

Among many other things, Wireless Sensor Networks (WSN) have been expanded thanks to the advances in technology and the price reduction of electronic components, which allows production of low-cost and low-power sensor nodes. Moreover, due to their ubiquity, the application of WSN covers many fields such as industrial, transportation, military, medical, environmental, agriculture, and others [1–3]. For many of the WSN applications, for instance, agricultural or environmental monitoring, the on-site interaction with the sensor node is quite limited for obvious reasons, thus, the sensor nodes must be designed in a manner that power consumption is optimized to make the sensor as autonomous as possible or even reach to a self-powered device [4].

In terms of hardware, several alternatives of low-power modules can be used to reduce power consumption: MEMS devices can be used for sensing; Zigbee, Bluetooth Low Energy (BLE), Low Power Wide Area (LPWA) for communications; low-power micro-controllers for processing and high-efficiency power management along with high capacity batteries for the power supply [4–6]. In addition, most of those component have inherited power-saving modes that may be used to reduce even more their power consumption. On the other hand, in terms of software, the efficient implementation of those power-saving modes would optimize their low-power capabilities. Moreover, if there is on-site data processing, the algorithms could be improved so that the controller requires lower resources to perform specific tasks.

For the case of noise pollution, there are several approaches of WSN developed, most of them based on low-cost hardware [7–10]. Although the low-power consumption requirement is always pointed out, there is a lack of specific strategies that help to achieve and evaluate the power consumption reduction in custom sensor nodes for acoustic measurements.

Thereby, the present paper proposes the hardware that may be used for a low-cost low-power acoustic sensor node (ASN) aimed to perform mobile noise measurements [11]. Then, to reduce the power consumption of the ASN's processing unit, two calculation methods of the one-third octave band spectrum (a task continuously executed), based on a Multi-rate Filter Bank and on the Power Spectral Density, are acoustically and electrically evaluated.

2. SENSOR NODE

A WSN is composed by many sensor nodes that are deployed throughout an area of interest. A sensor node consists mainly of the following subsystems [12]:

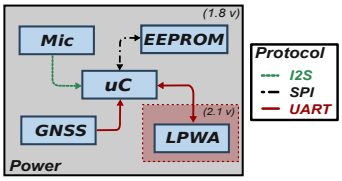

Figure 1: Main components of the ASN where two voltage domains are shown: 2.1 v for the LPWA and 1.8 v for the other modules. Moreover, the communication protocols between the uC and the other components are also shown.

- Controller/processing unit: Performs the data gathering, processing and tasks management.
- Sensing: Corresponds to the transducer(s) of physical signals to digital ones.
- Power supply/management: Provides the energy to the different subsystems of the sensor node.
- Communications: Transfers the gathered and preprocessed data. It is usually able to receive configuration commands of the sensor node as well.

2.1 Hardware design

For the case of acquiring mobile georeferenced noise measurements, the main components of the sensor are depicted in Figure 1, where the communication protocols between the modules and the processing unit, as well as their voltage supply, can also be observed. Thus, for the processing unit, the low-power microcontroller (uC) STM32L452RE was chosen. Moreover, the digital MEMS microphone SPH0645LM4H is selected for acquiring the acoustic signals. To perform the data georeferencing, the Global Navigation Satellite System (GNSS) MAX-M10S-00B is also included. Finally, to transmit the sampled data, the Low Power Wide Area (LPWA) SIMCOM SIM7022, which is complemented by the ultra-low power EEPROM module M95P32-IXMNT to temporary store samples when there is a lack of mobile network signal, are included as part of the communications unit. At the moment, the sensor node is powered by three AA batteries.

2.2 Processing unit tasks

The sampling, georeferencing and noise computation processes are based on [13], where a real-time operating system (FreeRTOS) keeps the tasks synchronized and concurrently executed to perform the georeferenced noise sampling. The major differences to the sensor proposed in [13] are the addition of wireless capabilities and the focus on low-power consumption so that the sensor node autonomy would be highly enhanced. Thus, the tasks and their description are as follows:

- **Sampling:** Acquires acoustic data continuously from the microphone at a sampling frequency of 32 kHz.
- **Signal processing:** It is executed every 125 ms (4000 samples). It computes the a-weighted and the one-third octave band equivalent sound levels ($L_{Aeq,\ 125ms}$ and $L_{eq-f_c,\ 125ms}$, respectively).
- **Georeferencing:** Computes the one second a-weighted and the one-third octave band equivalent sound levels, L_{Aeq} and L_{eq-f_c}, respectively. Then, the coordinates are obtained from the GNSS and all information is appended together in a local buffer.
- **Data transmission:** Once the local buffer has five L_{Aeq} and L_{eq-f_c}, after validating the network connection, it sends the data to the server (COAP protocol). In case that the mobile network is not available, a timeout is executed to try again after a given time. The timeout length is increased for each data transmission attempt in order to save energy.

2.3 Optimization

As mentioned before, another possibility to reduce the power consumption, specifically when a sensor node is continuously sampling/processing the measurements in real-time, is the optimization of the processing algorithms. Thus, to reduce the processing load in the signal processing task, which is executed continuously and with higher computation load, three algorithms will be evaluated for the calculation of the one-third octave band spectrum:

- Full filter bank (considered as the reference)
- Multi-rate filter bank (signal decimation)
- PSD

2.3.1. Full and multi-rate filter banks

Figure 2a shows a full filter bank for the calculation of the one-third octave spectrum, where one band-pass filter is employed. Moreover, Figure 2b shows a multi-rate filter bank, where a decimation filter is applied after three one-third octave bands to reduce the sampling frequency and, as a consequence, the number of samples to compute the one-third octave band spectrum. For the multi-rate filter, it is observed, based on the number of samples to be processed, that the computation should be reduced.

For the present comparison, to comply with Class 1 of IEC 61260-1:2014, the one-third octave filters are designed as 4^{th} order, for central frequencies 8 and 10 kHz, and 3^{rd} order, for central frequencies between 50 Hz and 6.3 kHz, Butterworth IIR pass-band filters, as recommended in literature [14].

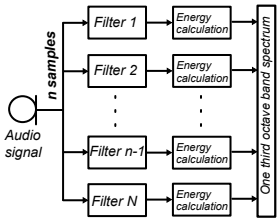

(a) Full filter bank

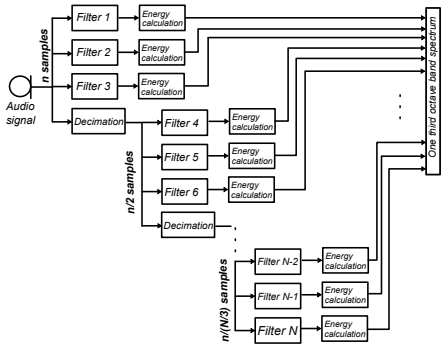

(b) Filter bank with decimation

Figure 2: Computation of one-third octave band spectrum based on filter banks: (a) full filter bank and (b) multi-rate filter bank (signal decimation every three filters).

2.3.2. Power spectral density (PSD)

An alternative to compute the one-third octave band spectrum is using the PSD, which provides the magnitude of the spectrum of the signal normalized to a 1 Hz band. For a discrete signal, and not including the DC component and the Nyquist frequency, the PSD is defined as:

$$PSD(k) = \frac{2\Delta t|X(k)|^2}{N}, \qquad 0 < k < N/2 \tag{1}$$

where $X(k)$ is the spectrum (FFT) of the input signal for the frequency bin k, N is the number of samples of the block and Δt is the sampling interval. For the optimal computation of the FFT, N is zero padded to reach 4096 samples (N_{zp}), thus:

$$k = \frac{Fs}{N_{zp}} = 7.8Hz. \tag{2}$$

Furthermore, to compute the one-third octave band spectrum, the $PSD(k)$ between the frequency band's lower (f_l) and upper (f_u) limits are summed and scaled to the current one-third octave band's bandwidth (Δf) as:

$$PSD_{f_c} = 10log_{10}\left\{\left[\sum_{k\epsilon[f_l,f_u)} PSD(k)\right]\Delta f\right\} \tag{3}$$

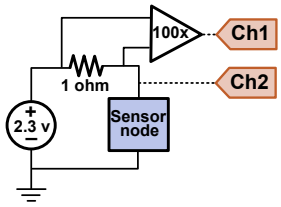

Figure 3: Schematic of current measurement based on a shunt resistor with a 100x voltage amplifier.

2.4 Methodology

Five ASNs are evaluated for both one-third octave band calculation algorithms (filter banks and PSD) in terms of the power consumption and acoustical performance. Since no wireless capabilities are required for the testing, the GNSS and LPWA modules are switched off. Also, no power-saving modes are implemented in the sensor node at this development stage.

2.4.1. Power consumption measurements

Figure 3 shows the schematic of the power consumption measurement of the ASN. A 1 ohm high precision shunt resistor, which is amplified 100 times by a high-performance operational amplifier in a differential configuration, is used to indirectly measure the current consumption using channel 1 of the Tektronix 2 series oscilloscope. Moreover, channel 2 is used to measure the input voltage simultaneously to compute the power consumption at each time t. Thus, based on the ohm's law, considering the 1 ohm resistance and the 100x voltage amplifier, the output of ch1 as a function of time can be converted to current as:

$$I(t) = \frac{V_{ch1}(t)}{100} \tag{4}$$

and the power consumption can be computed with:

$$P(t) = V_{ch2}(t) \times I(t) \tag{5}$$

for a measurement length of 2 seconds at a sampling frequency of 200 MHz of the oscilloscope.

Moreover, to contrast the power consumption between the three algorithms, the root mean square (RMS) was

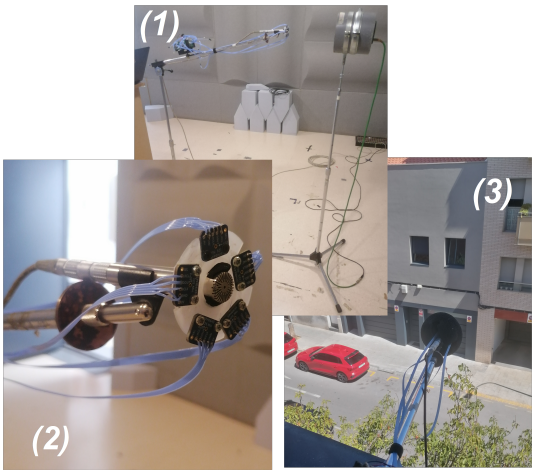

Figure 4: Acoustic testing set-up for laboratory tests and actual traffic noise measurements.

calculated for the whole period of measurement. Then, two comparisons are performed: one based on the actual power consumption (RMS) and the other using the power consumption normalized to the IDLE current ($\overline{RMS}$), that, from Equation 2.4.1 and the measured IDLE current (I_{idle}) is obtained as:

$$P_{norm}(t) = V_{Ch2}(t) \times [I(t) - I_{idle}] \tag{6}$$

2.4.2. Acoustic measurements

First, measurements are performed in a semi-anechoic chamber. A Beyma 5MP60N speaker with a frequency response from 50 to 12 kHz is placed at a height of 1.2 m in a tripod (Figure 4-1). Thereby, at an approximate distance of 20 cm, the 5 MEMS microphones of the sensor nodes, which are put around the microphone of a Type 1 Sound Level Meter (SLM) Cesva SC-310 using a plastic support in a pentagonal shape, are mounted in a tripod as well, with the microphone arrangement at the same height as the speaker (Figure 4-2). Then, three minutes of different sounds: white, pink and recorded noise traffic, are measured.

Second, 30 minutes of real traffic noise is measured at about six meters height through the opening of a window, as can be seen in Figure 4-3. A windshield was adapted to cover the microphone arrangement.

For the acoustic measurements, since one SLM is used as the reference, the tests are performed only for the optimized algorithms, i.e., the multi-rate filter bank and the

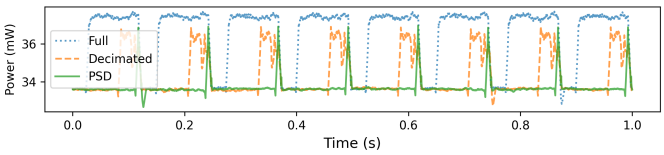

Figure 5: Comparison of the power consumption for the calculation of one-third octave band through full filter bank, multi-rate filter bank and PSD, for one ASN.

PSD. Thus, the one-third octave band noise level difference between the SLM and the average of the 5 ASNs is computed as:

$$\Delta L_{eq-f_c} = \frac{1}{5}\sum_{i=1}^{5} L^{i}_{eq-f_c} - L^{SLM}_{eq-f_c} \tag{7}$$

To observe the variability among different ANSs, the standard deviation σ_{f_c} is also computed considering the individual differences between the sensor nodes and the SLM.

3. RESULTS

3.1 Power consumption

Figure 5 shows an example of one second of power consumption measurement for one ASN and for the three calculation algorithms. It can be seen that, compared to the full filter bank, there is a clear power consumption reduction obtained for the optimized algorithms. Moreover, if one compares the multi-rate versus the PSD, it is observed that even more power consumption reduction is achieved, mainly because the one-third octave computation takes a shorter time to be completed since only one FFT is required instead of the 23 filters. Moreover, for the energy calculation of each one-third octave band, since for the filter bank the energy is computed based on the RMS of the filtered signal, the PSD requires less computation as well, as can be interpreted from Equation 2.3.2.

Table 1 shows the comparison of the average value (5 ASNs) of the RMS and the normalized one, $\overline{RMS}$. The percentage of power consumption reduction compared to the full filter bank is shown in parenthesis. It is observed that a general drop is obtained compared to the full filter bank. Moreover, the $\overline{RMS}$ shows the maximum power reduction that could be obtained using the implementation of the PSD, which is 88.4%. Since the proposed sensor node must be continuously taking acoustic samples, this maximum value could not be achieved in practice, but this

	Full bank [mW]	**Multi-rate** [mW]	**PSD** [mW]
RMS	39.62	37,48 (5.4)	36,98 (6.7)
$\overline{\mathbf{RMS}}$	3.07	0.97 (68.4)	0.36 (88.3)

Table 1: Power consumption comparison between the three algorithms for the computation of the one-third octave band spectrum. The RMS of the actual power consumption and the $\overline{RMS}$ normalized to the IDLE current is shown. The percentage of power consumption reduction compared to the full filter bank is shown in parentheses.

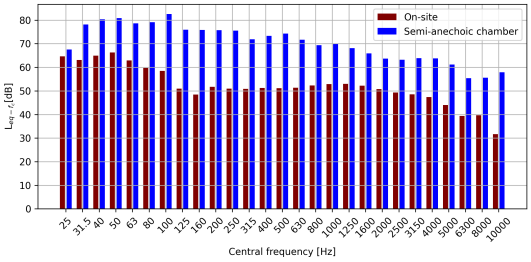

Figure 6: Comparison between the traffic noise measured on-site and in the semi-anechoic chamber.

result could be interpreted as the lower the IDLE current, the higher the contribution of the PSD algorithm to the energy saving.

3.2 Acoustical tests

Sub-figures 7a and 7b show the ΔL_{eq-f_c} of the multi-rate filter bank and the PSD algorithms, respectively. It is observed that in almost all of the frequencies for both algorithms, σ_{f_c} is lower than 1 dB, which means that the microphone arrangement (position) has no great influence in the results. Moreover, for the measurements performed in the semi-anechoic chamber, almost all of the ΔL_{eq-f_c} fall below 1 dB, except the two lowest frequencies in the white noise test for multi-rate filter bank and the two highest frequencies in traffic noise test for the PSD based algorithm.

Finally, for the case of the real traffic noise measurement, it can be seen that there is an overestimation of levels from 5 kHz and higher. This phenomenon, as can be seen in Figure 6, is mainly produced by the combination of the low noise levels measured for high frequencies, which are below 42 dB and corresponds the estimated linearity noise floor of the microphone, that also explains why it did not happen when using the speaker.

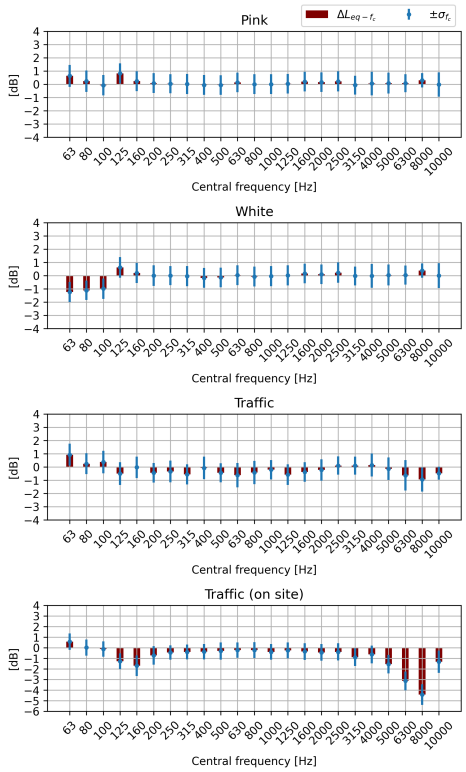

(a) Multi-rate filter bank

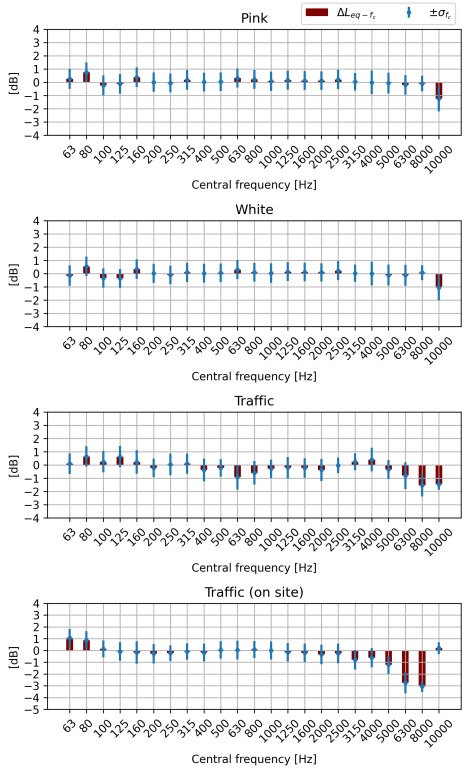

(b) PSD

Figure 7: Difference and standard deviation between the average L_{eq-f_c} of the ASNs and the one of the SLM for (a) the decimated filter bank and (b) PSD algorithms.

4. DISCUSSION

For the computation of the one-third octave band spectrum based on the PSD, it is important to note that since the frequency bins are for a fixed bandwidth (see Subsection 2.3.2), two one-third octave bands could share a frequency bin in some percentage. Different approaches could help to compensate for this issue such as assigning only the percentage belonging to each one-third octave band, which is not likely to highly increase the required processing. Moreover, due to the fixed and logarithmic frequency bandwidths of the PSD and one-third octave band, respectively, higher amount of bins (k) will be used to compute the energy (Equation 2.3.2) for higher frequency bands, thus, some uncertainty could be expected in lower frequencies for the short number of bins.

Moreover, regarding the required attenuation in [15], a comparison similar to the one show in this paper is presented in [14], the one-third octave band spectrum calculation through FFT and filter banks is acoustically compared, but with the aim of analyzing noise emitted by electrical substations. It was found that for specific frequencies, 31.5 Hz and 5 kHz, the attenuation levels as required by the normative [15] were not met. Moreover, when analyzing noise emitted by the substation, differences higher than 6 dB can be found. For the specific case of traffic noise analyzed in this paper, differences up to 4 dB were obtained mainly in high frequencies, but they are clearly explained by the combination of the low noise level of the source and the high noise floor of the MEMS microphone. Moreover, in mobile monitoring, the one-third octave measurement is used as a support to identify conflict situations, so the error in these bands, which does not affect the global value, is not critical.

5. CONCLUSIONS

The present study showed that implementing efficient algorithms could help to reduce the power consumption of the sensor nodes. Moreover, it was observed that having a low IDLE current of the ASN, which could be done by selecting proper hardware and managing their low-power modes efficiently, is also vital for achieving a greater power consumption reduction in terms of percentage due to these processing optimizations. Also, as seen in the results, the processing reduction due to the implementation of the one-third octave band spectrum calculation based on the PSD is superior to the ones based on filter banks, whether they are full or multi-rate (decimated).

For the case of the acoustic comparison, it is observed that both of the algorithms perform well for measuring common types of noises such as white, pink and traffic noise. The measured differences in the noise level of the ASNs compared to a Type 1 sound level meter fall most of the times below 1 dB. Moreover, although more tests are required to show it, a clear advantage of using the filter bank compared to PSD could not be observed in these preliminary tests.

REFERENCES

[1] M. Majid, S. Habib, A. R. Javed, M. Rizwan, G. Srivastava, T. R. Gadekallu, J. C.-W. Lin, Applications of Wireless Sensor Networks and Internet of Things Frameworks in the Industry Revolution 4.0: A Systematic Literature Review, Sensors 22 (6) (2022) 2087. doi:10.3390/s22062087.

[2] L. Hamami, B. Nassereddine, Application of wireless sensor networks in the field of irrigation: A review, Computers and Electronics in Agriculture 179 (2020) 105782. doi:10.1016/j.compag.2020.105782.

[3] P. C. Fiallos, J. R. Garbi, T. P. Gomez, LOW-COST DEVICE FOR FAULT DIAGNOSIS IN BEARINGS BASED ON THE HILBERT-HUANG TRANSFORM, DYNA 98 (5) (2023) 480–486. doi:10.6036/10875.

[4] R. A. Kjellby, L. R. Cenkeramaddi, A. Frøytlog, B. B. Lozano, J. Soumya, M. Bhange, Long-range & Self-powered IoT Devices for Agriculture & Aquaponics Based on Multi-hop Topology, in: 2019 IEEE 5th World Forum on Internet of Things (WF-IoT), 2019, pp. 545–549. doi:10.1109/WF-IoT.2019.8767196.

[5] D. Newell, M. Duffy, Review of Power Conversion and Energy Management for Low-Power, Low-Voltage Energy Harvesting Powered Wireless Sensors, IEEE Transactions on Power Electronics 34 (10) (2019) 9794–9805. doi:10.1109/TPEL.2019.2894465.

[6] S. Du, Y. Jia, S. Member, C. Zhao, A Nail-Size Piezoelectric Energy Harvesting System Integrating a MEMS Transducer and a CMOS SSHI Circuit 20 (1) (2020) 277–285, publisher: IEEE.

[7] P. W. Wessels, T. G. Basten, Design aspects of acoustic sensor networks for environmental noise monitoring, Applied Acoustics 110 (2016) 227–234, publisher: Elsevier Ltd. doi:10.1016/j.apacoust.2016.03.029.

[8] R. M. Alsina-Pagès, U. Hernandez-Jayo, F. Alías, I. Angulo, Design of a mobile low-cost sensor network using urban buses for real-time ubiquitous noise

monitoring, Sensors (Switzerland) 17 (1) (2017) 1–21. doi:10.3390/s17010057.

[9] C. Mydlarz, M. Sharma, Y. Lockerman, B. Steers, C. Silva, J. P. Bello, The Life of a New York City Noise Sensor Network, Sensors 19 (6) (2019) 1415, number: 6 Publisher: Multidisciplinary Digital Publishing Institute. doi:10.3390/s19061415.

[10] J. Picaut, A. Can, N. Fortin, J. Ardouin, M. Lagrange, Low-Cost Sensors for Urban Noise Monitoring Networks—A Literature Review, Sensors 20 (8) (2020) 2256. doi:10.3390/s20082256.

[11] G. Quintero, A. Balastegui, J. Romeu, Traffic noise assessment based on mobile measurements, Environmental Impact Assessment Review 86 (2021). doi:10.1016/j.eiar.2020.106488.

[12] K. Gulati, R. S. Kumar Boddu, D. Kapila, S. L. Bangare, N. Chandnani, G. Saravanan, A review paper on wireless sensor network techniques in Internet of Things (IoT), Materials Today: Proceedings 51 (2022) 161–165. doi:10.1016/j.matpr.2021.05.067.

[13] G. Quintero, A. Balastegui, J. Romeu, A low-cost noise measurement device for noise mapping based on mobile sampling, Measurement: Journal of the International Measurement Confederation 148 (2019) 106894. doi:10.1016/j.measurement.2019.106894.

[14] Z. Liao, Z. Gan, J. Hu, J. Zhao, B. Zhou, J. Zhang, Comparative study of two typical one-third octave algorithms in substation noise analysis, Energy Reports 8 (2022) 319–326. doi:10.1016/j.egyr.2022.10.156.

[15] IEC 61260-1:2014 | IEC.
URL https://webstore.iec.ch/publication/5063